A Wearable Self-Driven Piezoelectric Sensor Enabling Real-Time Blood Pressure Estimation

Ying Qian[1], Huimin Li[1], Anqi Li[1], Xinghui Liu[2], Guoxian Wu[2], Weikang Yu[2], Kai Wang[1,3]

[1]School of Electronics and Information Technology, Sun Yat-sen University, Guangzhou, China

[2] Shenzhen Chipwey Innovation Technologies Co.,Ltd , Shenzhen, China

[3]Guangdong Province Key Lab of Display Material and Technology, Sun Yat-sen University, Guangzhou,China

Email: wangkai23@mail.sysu.edu.cn (KW)

Abstract

In this article, a flexible wearable impulse wave sensor that utilizes a polyvinylidene fluoride(PVDF) film-type piezoelectric sensor and an a-Si:H dual-gate thin-film transistor as a buffer is reported. Differing from passive sensors, this active sensor provides signal rectification and amplification, and accurately collect the impulse wave signals with detailed characteristic peaks. We then propose an effective blood pressure estimation neural network method to obtain the blood pressure and extract parameters that are comparable to those from the model with the Advancement of Medical Instrumentation (AAMI).

Author Keywords

a-Si:H TFT; impulse wave sensor; blood pressure estimation

Introduction

Currently, wearable devices are divided into fitness wearable devices and medical wearable devices. In the medical field, wearable devices refer to flexible intelligent electronic devices that are easy to realize, early diagnosis and long-term monitoring in clinical and daily health activities. For flexible wearable sensor devices, there are still problems such as running time, portability, signal crosstalk, power consumption and real-time data transmission [1]. In addition, the accuracy of impulse wave sensor available for commercial wristband wearable devices is still insufficient and needs further improve [2].

The impulse wave signal is a physiological signal of the human body and it has been seriously considered to be used for monitoring cardiovascular health. In the early stages of certain cardiovascular diseases such as atherosclerosis, hypertension, and coronary heart disease, patients often do not have symptoms, but their blood flow and blood pressure might be abnormal. The impulse wave can be used to estimate heart rate and heart rate variability. By detecting and correctly identifying the time-domain characteristic points in the impulse waveform, cardiovascular disease prevention can be performed.

A typical impulse waveform has three characteristic peaks, and the important time-domain characteristics include the amplitude and time value of four characteristic points, namely the main wave, the pre-stroke wave, the descending isthmus and the dicrotic wave. The time-domain information of the main wave and the dicrotic wave is mainly used for calculating the blood pressure. The impulse wave signal is a non-stationary approximate periodic signal, which is mixed with baseline drift caused by breathing, AC power frequency interference, and some random interference induced by sampling equipment and sampling environment. The data obtained by the actual waveform collection has various changes, and there is also unavoidable human interference. It is necessary to use an algorithm corresponding to the impulse wave time-domain characteristic index for correct extraction.

The flexible sensor device can convert external deformation of the PVDF film into pulsed electrical signals. The piezoresistive sensing system has a simple device design and reading mechanism, low detection limit value, and fast response time [3], but there is a hysteresis effect which is a drawback [4]. Capacitive sensors can detect static force with low energy consumption in high sensitivity, but the response time is not as good as piezoelectric sensors [5]. The photoelectric volumetric sensing system based on the MEMS sensor array reduces the measurement time, but the quality of signal acquisition is related to the pressing pressure, and sensor calibration is required before usage [6]. The piezoelectric sensor based on the PVDF film has higher sensitivity and fast response speed. It can also attain lower power consumption and better linearity in the impulse beat detection. Xin Yi et al designed a "thin shell" structure impulse sensor system tied to the wrist, which improves the signal collection as compared with the planar structure, and conducts more sensitive and stable impulse wave acquisition [7].

In this paper, a dynamic impulse wave sensor based on piezoelectric film material PVDF and a-Si double-gate TFT (DGTFT) is proposed to rectify and convert the AC pulse signal into a DC current signal, and then use the amplification module and the acquisition module to collect the impulse wave data. In the end, we established a blood pressure prediction model by extracting the characteristic points of the impulse wave and calculating the corresponding blood pressure value to verify the availability of the pulse wave sensor for blood pressure estimation.

Device Architecture and Equivalent Circuit

In this paper, we designed a impulse wave acquisition system. As shown in Figure 1, the impulse wave acquisition system is composed of a PVDF film from MEAS company, a in-house fabricated dual-gate TFT and a ADA4530-1 Electrometer Amplifier from ADI. The ADA4530-1 Electrometer Amplifier is a fA-class input bias current amplifier, powered by ±5V. The amplifier uses the ADA4530-1 chip for cross-resistance amplification, the AD825 chip for voltage amplification and signal shielding measures for weak signal acquisition. The final output of the amplifier module is connected to the digital oscilloscope or upper computer to get pulse wave data. When collecting pulse wave, the PVDF is attached to the wrist, then the deformation caused by the pulse vibration stimulates the PVDF to generate the induced charge. After rectifying the signal by the dual-gate TFT and amplifying by ADA4530-1 amplifier module, the oscilloscope or the computer displays the impulse waveform.

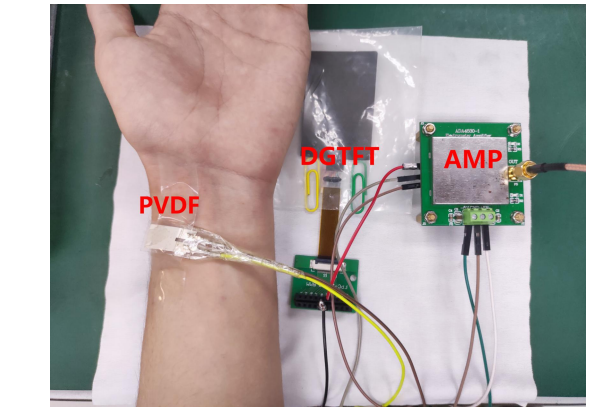

(a)

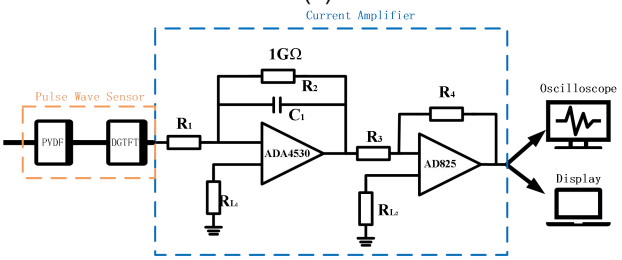

(b)

Figure 1. Experimental setup for measuring the pulse wave signal by the proposed integrated sensor module. (a) physical figure; (b) schematic diagram

The DGTFT working in the diode-like mode and the flexible polyvinylidene fluoride (PVDF) film form the detection part of the system. The PVDF film acts as the sensing component and the DGTFT is used as the rectifier. We designed and fabricated the a-Si:H dual-gate TFT by using a five-mask photolithographic fabrication process adopted from [8]. The dual-gate TFT is a four-terminal component, including a top gate(TG), a bottom gate(BG), a source(S) and a drain(D). The PVDF film is made of metal/PVDF/metal sandwich structure. One of the electrodes serves as the ground terminal(GND) and the other electrode serves as the charge sharing terminal(CST). For the impulse wave signal monitoring, the TG, BG and S of dual-gate TFT are shorted with the CST terminal and the source terminal (S) serves as an output terminal. For the pulse signal monitoring, the TG, BG and S of the dual-gate TFT are shorted and the source terminal (S) serves as an output terminal. In this case, DGTFT becomes a diode-connected TFT whose transfer characteristics is shown in Figure 2. It can be a replacement for a Schottky diode to rectify the signal.

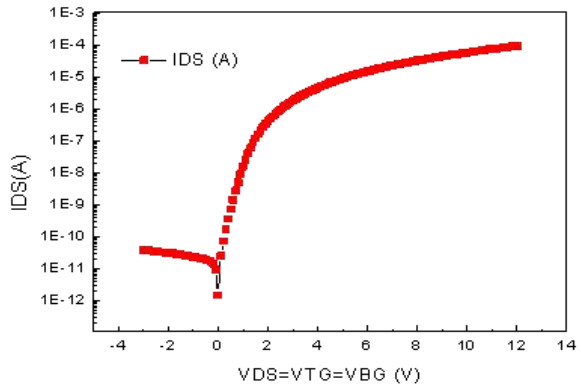

Figure 2. Transfer characteristics of the diode-like DGTFT (W/L=515/3μm)

The equivalent circuit of a monitoring system based on a pulse wave detector is shown in Figure 3. When the pulse force is applied, due to the piezoelectric effect of the piezoelectric PVDF [9-10], the force-induced charges come from both 31 and 33 directions, QPVDF is quantified as $d_{33} \cdot F_{33} + (L/T) d_{31} \cdot F_{31}$, where the applied force F_{33} and F_{31} in 33 and 31 directions, respectively. d_{33} and d_{31} are the piezoelectric coefficients. L and T are the length and thickness of the PVDF, respectively.

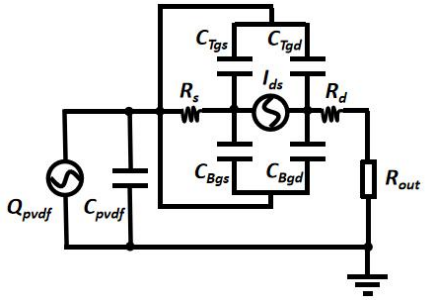

Figure 3. Equivalent circuit diagram of the PVDF-driven dual-gate TFT for pulse wave monitoring

Because there exists polarity between the charges generated by the PVDF film, the DGTFT works in both ON state and OFF state, and only passes forward current. Considering C_{Pvdf} as the PVDF capacitance, C_{Top} as the top gate capacitance, C_{Bottom} as the bottom gate capacitance, and $C_{Channel}$ as the channel capacitance, and neglecting parasitic capacitances C_{Tgs}, C_{Tgd}, C_{Bgs} and resistances R_s and R_d, the drain-source voltage V_{DS} of the DGTFT is equal to V_{BG} and V_{TG}

$$V_{TG} = V_{BG} = V_{DS} = \frac{Q}{C_{Total}} = \frac{d_{33}F_{33} + \frac{L}{T} d_{31}F_{31}}{C_{Pvdf} + C_{Top} + C_{Bottom} + C_{Channel}} \quad (1)$$

The DGTFT differs from the conventional TFT in that its threshold voltage is adjustable through biasing the top gate and the bottom gate, respectively. The threshold voltage V_T is therefore modeled as $V_T = V_{T0} - \gamma V_{TG}$, where V_{T0} is the threshold voltage of the DGTFT under zero force applied to the PVDF and γ is the dependence parameter, showing how V_T depends on V_{TG} [10].

Since the force generated by the impulse is generally weak and therefore, the bottom-gate bias is much smaller than the threshold voltage but greater than zero. Hence, the device works in the deep sub-threshold regime and the output current (I_{DS}) is given as below

$$I_{DS} = I_{D0} \exp\left(\frac{q[(1+\gamma)V_{TG} - V_{T0}]}{\beta \cdot kT}\right) \times \left[1 - \exp\left(\frac{-q \cdot V_{DS}}{kT}\right)\right] \quad (2)$$

$$= I_{D0} \exp\left(\frac{q\left[(1+\gamma)\left(\frac{d_{33}F_{33}}{C_{Pvdf} + C_{Top} + C_{Bottom} + C_{Channel}}\right) - V_{T0}\right]}{\beta \cdot kT}\right)$$

$$\times \left[1 - \exp\left(\frac{-q \cdot \left(\frac{d_{33}F_{33}}{C_{Pvdf} + C_{Top} + C_{Bottom} + C_{Channel}}\right)}{kT}\right)\right]$$

Where, I_{D0} drain-source output current at $V_{BG} = V_{TH}$ and for $V_{DS} >> kT/q$, q is the electron charge, k is Boltzmann constant, T is the absolute temperature in Kelvin, S is a subthreshold swing and β is related to S as $\beta = qS/(kT\ln 10)$. The impulse force on the PVDF mainly generates the transversal mechanical stress and thus making piezoelectric charges in the d_{31} direction negligible.

Blood Pressure Estimation

The response of the impulse wave sensor in the form of the voltage signal from the impulse at the wrist of the human body is shown in Figure 4. Before the start of the experiment, the volunteer sat quietly for five minutes to keep breathing steadily. The obtained impulse waveform shows clearly the characteristic peaks: the main wave (ABC) and the dicrotic wave (CDE). The signal increases and decreases as the volunteer's heart contracts and dilates, respectively. When the heart contracts, aortic vessels appear elastic dilation, making the DGTFT experience an elevated force and leading to a signal increase. Contrarily, the aorta close when the heart was diastolic, driving the DGTFT to experience a decreased force, thus resulting in the decrease of the output voltage. Thus, the impulse wave sensor can accurately extract the pulse wave signals.

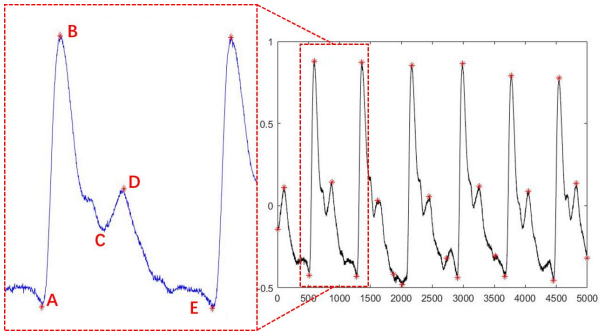

Figure 4. The original impulse waves obtained from the sensor

Furthermore, a series of experiments were performed to collect the data and validate the availability of the sensor for blood pressure estimation. We established a database contains 10 volunteers' records and used the MIMIC-II database [11] to build a blood pressure estimation model. The model architecture is showed in Figure 5. We first implement preprocessing for the pulse wave signals, including low-pass filtering, baseline drift processing, signal segmentation and interpolation [12]. After a series of above-mentioned processing, we obtained a large number of segments consisting of five periods of the pulse wave with a total of 625 data points. The comparison before and after preprocessing is shown in Figure 6. Through sufficient training, an effective blood pressure estimation neural network was established. To validate the performance of the network, the results of the model were compared to the Association for the Advancement of Medical Instrumentation (AAMI) standard [13]. The comparison of the result is represented in Table 1. As evident in Table.1, the algorithm performs well and meets the requirements of AAMI. Table 2 represents the measurement of some volunteers and analyzes the relative error of the model results and the measurement results of the electronic blood pressure monitor which is regarded as the actual blood pressure. The result showed the estimated blood pressure was very close to the actual blood pressure which indicated that the blood pressure of the monitored individual can be acquired by the impulse wave sensor together with blood pressure estimation method.

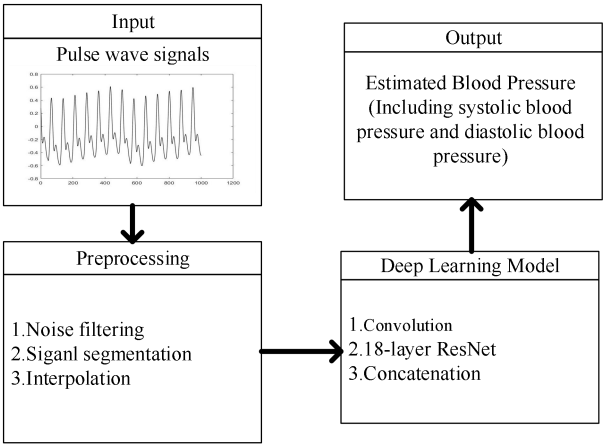

Figure 5. Algorithm framework diagram

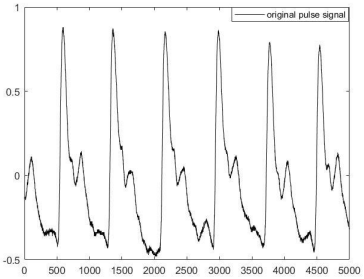

(a)

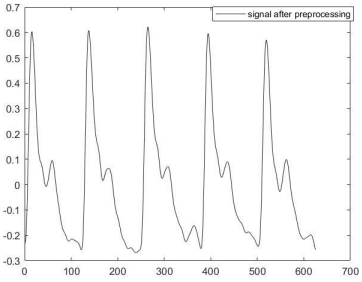

(b)

Figure 6. (a) the original impulse wave; (b) the impulse wave after processing

Table 1. Evaluation compared to the AAMI.

	SBP		DBP		Subjects
	MD	STD	MD	STD	
Proposed Estimation Model	2.1222	7.2619	-3.4175	5.1986	>85
AAMI	≤5	≤8	≤5	≤8	>85

Table 2. The model prediction results

	Estimation Model (mmHg)		Electronic Sphygmomanometer (mmHg)		Absolute Relative Error (%/%)
	SBP	DBP	SBP	DBP	SBP/DBP
1	98.961845	62.168476	107.0	70.0	7.51/11.18
2	121.00563	71.49375	126.0	72.0	3.96/0.70
3	123.40524	72.29983	116.0	77.0	6.38/0.60
4	115.76511	84.25687	115.0	78.0	0.66/8.02
5	112.37256	85.61182	120.0	80.0	6.36/7.01
6	91.73893	62.59045	104.0	70.0	11.78/10.59
7	107.71958	63.86951	108.0	68.0	0.26/6.07
8	134.6419	71.3283	125.0	75.0	7.71/4.89
9	116.58977	56.66023	113.0	58.0	3.18/2.31
10	120.13783	67.51562	114.0	77.0	5.38/12.32

Conclusion

A wearable self-driven piezoelectric sensor for blood pressure estimation was proposed and studied, and a blood pressure estimation model was established based on the MIMIC-II database. In terms of MD ±STD, the model achieves an overall accuracy of 2.12±7.26 mmHg for SBP and -3.42±5.20 mmHg for DBP, all of which meet the AAMI standards.

References

1. Hyo Young Lim, Kim H S, Qazi R, et al. Advanced Soft Materials, Sensor Integrations, and Applications of Wearable Flexible Hybrid Electronics in Healthcare, Energy, and Environment[J]. Advanced Materials, 2020:1901924.
2. Anna S, Mattsson C, Daryl W, et al. Accuracy in Wrist-Worn, Sensor-Based Measurements of Heart Rate and Energy Expenditure in a Diverse Cohort[J]. Journal of Personalized Medicine, 2017, 7(2):3.
3. Choong C L, Shim M B, Lee B S, et al. Highly Stretchable Resistive Pressure Sensors Using a Conductive Elastomeric Composite on a Micropyramid Array[J]. Advanced Materials, 2014, 26(21):3451–3458.
4. He J, Zhang Y, Zhou R, et al. Recent advances of wearable and flexible piezoresistivity pressure sensor devices and its future prospects[J]. Journal of Materiomics, 2020, 6(1): 86-101.
5. Lee B Y, Kim J, Kim H, et al. Low-cost flexible pressure sensor based on dielectric elastomer film with micro-pores[J]. Sensors and Actuators A Physical, 2016, 240:103-109.
6. Kaisti M, Panula T, Leppnen J, et al. Clinical assessment of a non-invasive wearable MEMS pressure sensor array for monitoring of arterial pulse waveform, heart rate and detection of atrial fibrillation[J]. npj Digital Medicine, 2019, 2(1):39-.
7. Xin Y, Qi X, Qian C, et al. A wearable respiration and pulse monitoring system based on PVDF piezoelectric film[J]. Integrated Ferroelectrics, 2014, 158(1): 43-51.
8. W. Li, C. Lin, A. Rasheed, E. Iranmanesh, Q. Zhou and K. Wang, "A Force and Temperature Sensor Array Based on 3-D Field-Coupled Thin-Film Transistors for Tactile Intelligence," in IEEE Transactions on Electron Devices, vol. 67, no. 7, pp. 2890-2895, July 2020, doi: 10.1109/TED.2020.2995582.
9. OoJ. G. Smits, S.I. Dalke, and T.K.Cooney, “The constituent equations of piezoelectric bimorphs,” Sensors and Actuators A, vol. 28, pp.41-61, 1991
10. E. Iranmanesh, A. Rasheed, W. Li and K. Wang, "A Wearable Piezoelectric Energy Harvester Rectified by a Dual-Gate Thin-Film Transistor," in IEEE Transactions on Electron Devices, vol. 65, no. 2, pp. 542-546, Feb. 2018, doi: 10.1109/TED.2017.2780261.
11. Raffa, J. (2016). Clinical data from the MIMIC-II database for a case study on indwelling arterial catheters (version 1.0). PhysioNet. https://doi.org/10.13026/C2NC7F.
12. Miao F, Wen B , Hu Z , et al. Continuous Blood Pressure Measurement from One-Channel Electrocardiogram Signal Using Deep-Learning Techniques[J]. Artificial Intelligence in Medicine, 2020:101919.
13. American National Standard for Electronic or Automated Sphygmomanometers, ANSI/AAMISP102002,Arlington,VA,USA:Association for the Advancement Instrumentation, 2002.